Table 1. Parameters used in simulation

Symbol	value
c_1	1.35×10^{-9} m^3 J^{-1}
c_2	3.44×10^{-24} Pa^{-3} s^{-1}
c_3	4.05×10^{-2} m$^{9/4}$ Pa$^{-1/2}$ s^{-1}
k_{leak}	0
n	3
α	5/4
β	3/2
ρ_i	910 kg m^{-3}
ρ_w	1000 kg m^{-3}
g	9.8 m s^{-2}
S_{PR}, S_{PK}	2.65×10^{-3} m^2
S_{R0}, S_{K0}	3.32 m^2
uh_R, uh_K	3.47×10^{-6} m^2 s^{-1}
T	1
n_c	2
V_p	2.53×10^{-5} m^3 Pa^{-1}

5.2 Model results

Network-based models for drainage channelization (e.g. Schoof (2010); Hewitt (2013); Werder et al. (2013)) have been used previously to model the seasonal evolution of drainage systems. In particular, they have been used to model the evolution of a channelized system from a more spatially extensive one as in stages 1 and 2 identified in this paper, and the subsequent shut-down of the system as in stage 3. See for instance figure 3 of Schoof (2010), figure 5 of Hewitt (2013), and figure 12 of Werder et al. (2013) for examples of seasonal drainage evolution. What these models are missing is the ability to capture the formation of disconnected regions at the glacier bed and the subsequent ability of parts of the bed to connect and disconnect to the drainage system, which is what we focus on here.

Instead of attempting to model a full seasonal cycle, we focus here on the effect of time-dependent water input into a fully channelized drainage system, in order to test whether our modification of existing models can capture the qualitative behaviour of the switching events such as those in Fig. 10 (see in particular panel g). In other words, we focus on the behaviour of the drainage system in stage 2. Our simulation is an idealized run, not based on the specific geometry or properties of the South Glacier field site and does not claim to reproduce observations beyond their generic features. Work to use proxies for surface melt rates and likely surface water supply routing in an inverse model for the drainage system is currently underway and will be reported elsewhere. Our aim here is simply to study the qualitative features of a forward model modified from existing ones found in the literature.

The rectangular domain is 5 km long and 1 km wide. The ice and bed surfaces are used with contour lines in panels c and g of Fig. 16, where black lines are surface contours at 100 m intervals, and grey lines are bed contours at the same intervals. Zero inflow is prescribed at the sides and top of the domain, and zero effective pressure at the lower end of the domain $y = 0$. The network geometry is the same as indicated in Fig. 1 of the supplementary material to Hewitt (2013), with a total of 201×201 nodes.

We allow water to be supplied in 40 discrete locations (effectively, moulins). Each moulin undergoes a diurnal cycle whose amplitude varies over several days, with mean water supply rates also varying over several days; the dominant period of the cycle is the same for each moulin but the ratio of diurnal amplitude to mean water supply is chosen randomly (while maintaining positive water supply rates at all times), and we have allowed for slight phase shifts between moulins. The time series of water supply to all moulins are shown in Fig. 16i.

We show two different simulations. Both use the parameter values shown in table 1, except that the percolation cut-offs S_{PR} and S_{PK} that have been set to zero in the first simulation, and uh_R and uh_K are set to one tenth the value given in table 1. Figure 16 shows one set of panels for each simulation, identified by the numbers 1 (no percolation cut-off) and 2 (finite percolation cut-off) in the panel labels. When referring to a specific panel for both simulations at the same time, we will identify it by the letter in the panel label. Both simulations start from a fully channelized steady state computed with moulin water supply set to constant values. Diurnal oscillations are subsequently superimposed on those constant water supply values. The system is run for several days to account for transients before the detailed results shown in Fig. 16 are computed.

The channelized configuration of the system does not change during the simulation (compare panels a and e in Fig. 16), although it differs slightly between the two simulations. Pressure oscillations result from the time-dependent water supply. These pressure variations are confined to the connected drainage system (compare panels c and g of 16, and see also the supplementary movie #2). In the second simulation (with non-zero percolation cut-offs), the extent of connected drainage system also evolves, shown as blue areas in panels d2 and h2 of Fig. 16 and the supplementary movie #2. While pockets of water can move down-glacier essentially without connection to the channelized system (see the left-hand side of the main drainage axis in supplementary movie #2), the main feature here is the expansion of the connected system at times of large water supply and low effective pressures. The larger connected system in panel h2 of Fig. 16 corresponds to peak water supply, the smaller system in panel d2 to the minimum water supply in the cycle shown. This is at least qualitatively consistent with our observation of switching events, that establish connectivity during periods of increasing water supply.

In Fig. 17, we focus on what an array of boreholes would observe. The borehole array is located in the black rectangle shown in Fig. 16 panel d2. Panels a2-c2 in Fig. 17 show the evolution of the connected parts of the bed within the borehole array, while panels d2-g2 show pressure time series, again grouped subjectively. The presence of at least two distinct drainage subsystems is immediately obvious (circles and diamonds in panels a2-c2, corresponding to series shown in panels d2 and e2 respectively). These two subsystems correspond to two different drainage channels. The grouping of boreholes in panel f2 (triangles) is intermittently connected to the diagonal channel of panel e2 (diamonds), with different boreholes connecting and disconnecting at different times, though connection and disconnection are again typically favoured by low and high effective pressures, respectively. This is in qualitative agreement with our actual borehole data (see Fig. 10g). In addition, there is an

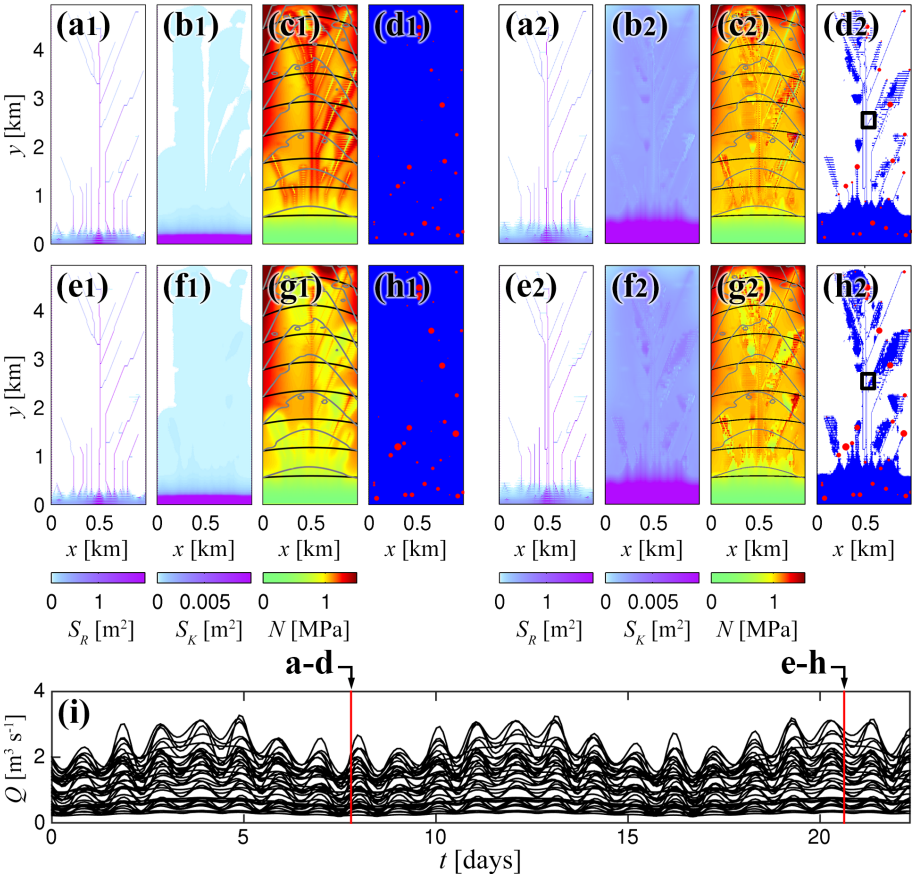

Figure 16. Snapshots of drainage system evolution for the model without a percolation cut-off (left), and with it (right). Panels a & e: S_R conduit size. Panels b & f: S_K conduit size. Panels c & g: effective pressure, black lines are 100 m surface contours, grey lines 100 m bed contours. Panels d & h: connectedness of conduits, indicated in blue if $S_{R,ij} > S_{PR}$ or $S_{K,ij} > S_{PK}$ along a given edge, in white otherwise. Red dotes indicate moulin locations, size of dot scaled with instantaneous water supply. Row a-d show solutions at t = 7.8 days and row e-h at t = 20.6 days. Panel i: water supply time series for all moulins in the domain.

additional grouping of persistently disconnected boreholes (Fig. 17 panel g2, crosses), although two of these become very poorly connected later in the cycle, permitting an excursion in effective pressure without obvious diurnal cycling.

One important aspect of the synthetic borehole records in panel f2 of Fig. 17, is the relatively minimal attenuation of amplitude and minimal phase lags observed within that distributed system relative to the channel (panel e2) to which the distributed system connects, and the abrupt switching to nearly constant effective pressures on disconnection. Compared with borehole data from South Glacier, we do not reproduce the tendency of disconnected boreholes to experience rising water pressure (i.e. falling effective pressure), which we believe is related to the dynamics of isolated boreholes incised upwards into the ice being squeezed by anisotropic stresses in the ice, an effect this drainage model is not designed to capture.

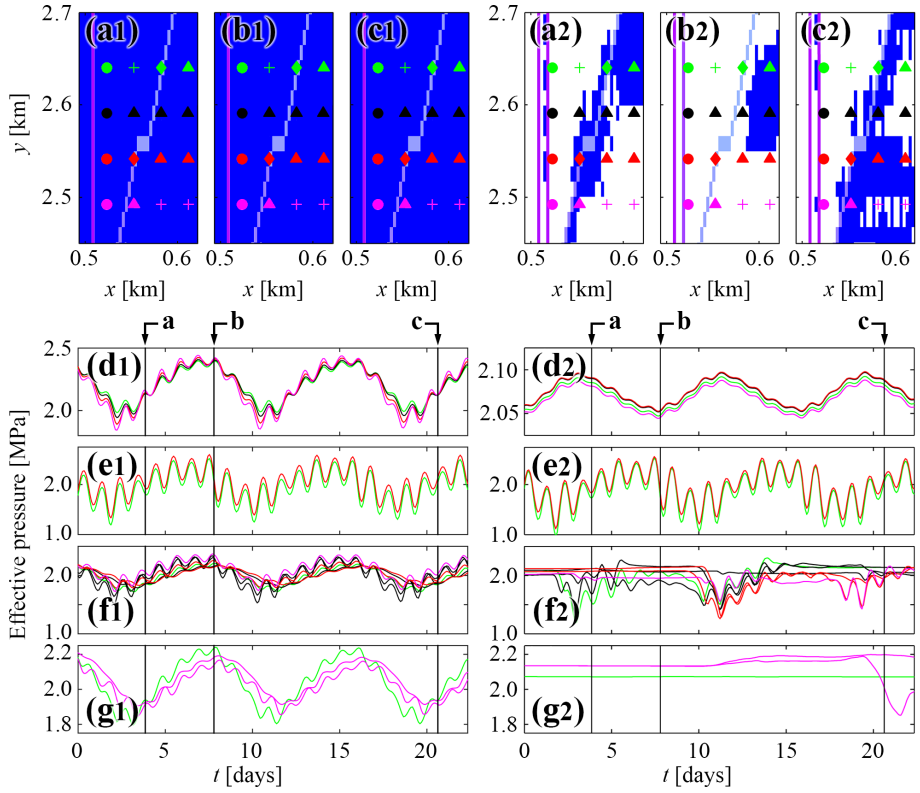

Figure 17. A synthetic borehole grid in the model without a percolation cut-off (left), and with it (right). (a–c): enlargements of the inset box in Fig. 16(d2,h2) at times t = 3.9 (a), 7.8 (b) and 20.6 (c) days. Superimposed on the blue connectivity map is S_R conduit size, plotted using the same colour scheme as indicated by the colour bar in panels a & e in Fig. 16 . Also shown are the locations of 16 synthetic boreholes, colour-coded by row, (d–g). Effective pressure time series from the boreholes, grouped according to borehole symbols: circles (d), diamonds (e), triangles (f), crosses (g). Each time series is colour-coded by row.

Removing the percolation cut-off increases the ability of the distributed system to drain water (equations 4 and 5). To account for this we simultaneously lower conduit opening rates uh_R and uh_K to $3.47 \times 10^{-7} m^2 s^{-1}$, keeping all other parameters the same, and then impose the same oscillatory melt input in Fig. 16. In order to create comparable drainage structures in both simulations, simulation 1 was started from the same initial state as simulation 2. The percolation cut-offs and conduit opening rates were then gradually changed with water supply rates held constant until a new steady state was achieved, before imposing diurnal oscillations again. A small change in channel configuration also results from removing the percolation cutoffs: two of the main drainage channels along the centre of the glacier in Fig. 16 panels a2 and e2 collapse onto a single channel in panels a1 and e1, as they are no longer isolated from each other by the percolation cut-off. The main difference in model results is however the much larger region over which the effect of oscillatory water input is felt away from the channels (compare Fig. 16 panels c1 and g1 with panels c2 and g2). This is a natural consequence of enforcing connectivity in the drainage system everywhere (see Fig. 16 panels d1 and h1).

In left side of Fig. 17 we use the same groupings picked from the simulation with percolation cut-off (right side). The boreholes marked as diamonds produce an almost identical pressure time series as in the first simulation (compare panels e1 and e2 in Fig. 17), indicating that the behaviour of channelized drainage is not substantially affected by dispensing with the percolation cut-off. By contrast, the boreholes marked as circles in Fig. 17 experience higher mean effective pressures and bigger oscillations in panel d1 than d2. This is the result of the two channels on the left-hand edge of the domain in Fig. 17 panels a2-c2 been merged into a single channel in panels a1-c1: the percolation cut-off allows subsystems to co-exist separately in closer proximity, in accordance with our observations at South Glacier.

The biggest difference is in the behaviour of the boreholes within the distributed system surrounding the channels (Fig. 17 panels f and g). Unlike in the case of the model with a percolation cut-off, the results in panels f1 and g1 no longer exhibit switching events, and there are no persistently disconnected boreholes. Instead, we see evidence of typically diffusive behaviour away from the channels: a reduction in the amplitude especially of the higher frequency (diurnal) forcing components with an attendant phase shift, and the absence of a sharp division between drainage subsystems. This behaviour mimics that in Fig. 8 of Werder et al. (2013), but contrasts with our field observations. Those observations indicate minimal variations in amplitude and phase shifts within drainage subsystems, with sharp boundaries separating different subsystems. The inability to explain those features of our field observations motivates the model modification we have proposed here.

That modification comes with one major drawback, which we do not attempt to resolve here. While the model is able to open drainage connections spontaneously, this is a slow process driven by viscous deformation, controlled by the non-local effective pressure term in equation 8. When the drainage system is subject to a rapid increase in water supply, the physics by which drainage connections are established may involve either elastic hydrofracture driven by overpressurization (e.g. Tsai and Rice (2012)) or the large-scale uplift of ice at flotation as described in Schoof et al. (2012). As we discuss in the supplementary material, the latter is not straightforward to incorporate into our modified model, as is the former (which requires a blending of elastic and viscous effects). We identify this as an important area for future research.